RESEARCH ARTICLE

NANO · MICRO small
www.small-journal.com

Organic Electrolyte Additive: Dual Functions Toward Fast Sulfur Conversion and Stable Li Deposition for Advanced Li–S Batteries

Yahui Liu, Kuikui Xiao, Shuo Yang,* Jiangdong Sun, Shirui Li, Xi Liu, Dong Cai, Yinhang Zhang, Huagui Nie,* and Zhi Yang**

Lithium—sulfur (Li–S) battery is of great potential for the next generation energy storage device due to the high specific capacity energy density. However, the sluggish kinetics of S redox and the dendrite Li growth are the main challenges to hinder its commercial application. Herein, an organic electrolyte additive, i.e., benzyl chloride (BzCl), is applied as the remedy to address the two issues. In detail, BzCl can split into Bz· radical to react with the polysulfides, forming a Bz–S–Bz intermediate, which changes the conversion path of S and improves the kinetics by accelerating the S splitting. Meanwhile, a tight and robust solid electrolyte interphase (SEI) rich in inorganic ingredients namely LiCl, LiF, and Li_2O, is formed on the surface of Li metal, accelerating the ion conductivity and blocking the decomposition of the solvent and lithium polysulfides. Therefore, the Li–S battery with BzCl as the additive remains high capacity of 693.2 mAh g^{-1} after 220 cycles at 0.5 C with a low decay rate of 0.11%. This work provides a novel strategy to boost the electrochemical performances in both cathode and anode and gives a guide on the electrolyte design toward high-performance Li–S batteries.

1. Introduction

Li–S battery is regarded as the most potential candidate for the next-generation energy storage device due to the high theoretical energy density of 2600 Wh kg^{-1}.[1–4] S cathode and Li metal anode deliver ultrahigh theoretical capacities of 1675 and 3680 mAh g^{-1}, respectively. Additionally, the low cost (300 $ per ton), non-toxic of S, and low equilibrium potential of Li (−3.04 V vs the standard hydrogen electrode) further contribute to the fast development of the Li–S battery.[5,6] However, the commercialization of Li–S battery is struggling due to the drawbacks of both S cathode and Li metal anode.[7] For the S cathode, the dissolution of the soluble lithium polysulfides (LiPSs, Li_2S_n, $4 \leq n \leq 8$), the poor electric conductivity of Li_2S_2 and Li_2S and the sluggish kinetics of the phase transition (solid–liquid–solid) are the main concerns.[8] For the Li metal anode, the unstable interphase of Li metal further deteriorates the reversibility and results in electrolyte consumption.[9–11]

Over the past years, numerous strategies have been devised in Li–S battery to engineer the S cathode and Li metal anode,[12,13] including: 1) electrode construction, such as confining S/Li in various substrates with 3D structure to alleviate the diffusion of soluble LiPSs, accelerate the S conversion and accommodate the volume change of S/Li; 2) interphase modification, including constructing separator or create a new path for the S transition, meanwhile, solve the problems in the Li metal anode. 3) Electrolyte optimization, such as regulating the dissolution of LiPSs and accelerating Li ion transport by altering the solvents and/or Li salts.[14,15] Notably, the electrochemical process of S cathode is a complex process that involves multiple conversions and multiphase transformations,[16] among which, the conversion kinetics from Li_2S_4 (liquid) to Li_2S_2/Li_2S (solid) is especially limited and regarded as the rate-determining step.[17–19] While the previous methods are mainly focused on the external regulation by improving the adsorption through S or Li atoms in LiPSs, the critical step is not the primary consideration, and the issues of Li anode are not resolved simultaneously.[20,21] Thus, it is essential to exploit a novel method to accelerate the specific step from Li_2S_4 to Li_2S_2/Li_2S, or create a new path for the S transition, meanwhile, solve the problems in the Li metal anode.

Electrolyte engineering is a feasible way to affect the performance of Li–S battery, as it can interact with LiPSs as well as Li metal.[22,23] Some electrolyte additives, such as 1,3,5-benzenetrithiol (BTT), methyl trifluoroacetate (CH_3TFA), and SnI_4 have been reported to participate in the S conversion and involve in the SEI formation on the Li metal anode.[24–26] Among the additives, organics arouse the researchers attention due to the tunable groups of the organic molecules, which provide the

Y. Liu, K. Xiao, S. Yang, J. Sun, S. Li, X. Liu, D. Cai, Y. Zhang, H. Nie, Z. Yang
Key Laboratory of Carbon Materials of Zhejiang Province
Wenzhou University
Wenzhou 325035, China
E-mail: 20220125@wzu.edu.cn; yangshuo@wzu.edu.cn; niehuagui@wzu.edu.cn; yang201079@126.com
S. Yang
College of Electrical and Electronic Engineering
Wenzhou University
Wenzhou 325035, China

The ORCID identification number(s) for the author(s) of this article can be found under https://doi.org/10.1002/smll.202309890

DOI: 10.1002/smll.202309890

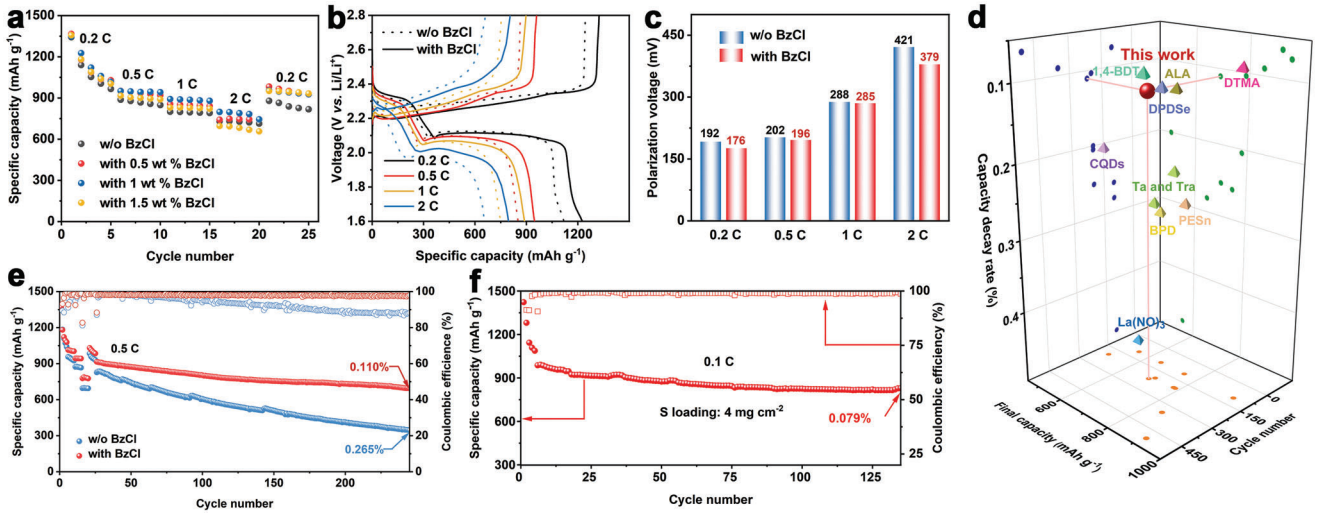

Figure 1. a) The rate performance of the cells with 0, 0.5, 1, and 1.5 wt% BzCl additive. b) Charge/discharge curves of the cells without (dotted line) and with (solid line) 1 wt% BzCl at 0.2, 0.5, 1, and 2 C. c) The voltage difference (ΔE) between the platforms in charge and discharge processes. d) Performance comparison to different additives reported previously (The detailed values are presented in **Table** S1, Supporting Information). e) The long cycling performance of cells at 0.5 C without and with 1 wt% BzCl. f) The cycling performance of Li–S cell with 1 wt% BzCl under a S mass loading of 4 mg cm^{-1}.

property with perspective possibilities.[27–29] For example, BTT was employed as a dual functional additive, where the S atom in BTT can form S—S bond with the LiPSs to change the redox path of S and form S—Li bond on the SEI to suppress Li dendrite growth.[24,30] CH_3TFA was also investigated as an additive in Li–S battery, and the results showed that the dimethyl polysulfides formed by the chemical reaction between methyl group in CH_3TFA and LiPSs, which is beneficial for the solubility of intermediate species, meanwhile, TFA anion can interact with Li-ion to form LiTFA, which improves the discharge kinetics.[25] Although certain progress has been achieved in the development of high-performance Li–S battery, the mechanism and specific reaction path with the organic molecule additive is lack of sufficient evidence, and the establishment of a lower-cost and diversiform organic molecules is still challenging.[31,32] Among the organic molecules, benzyl halide draws the attention because the benzyl group is a significant intermediate phase during the formation of organic materials, and benzyl free radical (Bz·) is expected to be formed and react with the LiPSs during the electrochemical process. Meanwhile, halogen is easily detached from the organic subject, which provides the space for the interaction between Bz· and polysulfides. In addition, the detached halogen can be involved in the formation of the ideal SEI with Li—X (X = F, Cl, I), which is a high Li ion conductor. In previous report, benzyl chloride (BzCl) has been investigated to react with S species to form sufficiently stable benzylized S species.[33] Motivated by these issues, BzCl is selected as an electrolyte additive to work as the LiPSs conversion accelerator and Li dendrite inhibitor.

Herein, with systematically electrochemical measurements together with full characterizations, BzCl is proved to improve the Li–S battery in two aspects: 1) Bz· radical from the BzCl is able to grab the S atom from the LiPSs to form Bz–S–Bz as an intermediate, and convert to Li_2S directly, which accelerates the conversion of the S species; 2) a flat and robust SEI which is rich in LiCl, LiF, and Li_2O covers the Li metal uniformly, constructing a high stable and ion conductive interphase. The results show that the Li–S battery with BzCl as an electrolyte additive delivers an improved performance of 787 mAh g^{-1} at the current density of 2 C, and maintains the high capacity retention of 75.8% in 220 cycles. This strategy expands the selectivity of the organic molecules to design fast S kinetics and reversible interfacial chemistry, and gives a guide to the mechanism for the organic molecules in Li–S battery.

2. Result and Discussion

2.1. Electrochemical Performance of BzCl Electrolyte in Li–S Batteries

The impact of BzCl additive on the electrochemical performance was first evaluated by carrying out galvanostatic measurements on the corresponding Li–S cells. For optimizing the concentration of BzCl with 69.2 wt% of S content (Figure S1, Supporting Information). The electrolytes with various concentrations of BzCl (0, 0.5, 1, and 1.5 wt%) were added to the cells and tested at different current densities, as shown in **Figure** 1a. The results prove that the cell with 1 wt% BzCl presents the highest capacity. Thus, the concentration of BzCl was set to 1 wt% in the following electrochemical tests. Relatively high capacities of 1347, 950, 891, 798, and 954 mAh g^{-1} are achieved in the Li–S cell with BzCl at 0.2, 0.5, 1, 2, and 0.2 C, respectively, whereas the values are 1342, 887, 800, 729, and 879 mAh g^{-1} for the cell with standard electrolyte. The charge/discharge curves of the two cells under different rates are compared and displayed in Figure 1b. It is clear to see that cell with BzCl shows more flatted plateaus on the second discharge curve, especially at the state of larger current density (>0.5 C), demonstrating that the conversion of the Li_2S_4 to Li_2S_2/Li_2S is more efficient and thorough with the help of BzCl additive. Meanwhile, the voltage differences (ΔE) between the charge and discharge platform are much smaller in the cell

using BzCl as additive (Figure 1c), which are 176, 196, 285, and 379 mV at 0.2, 0.5, 1, and 2 C, respectively, while those in the cells without additive are 192, 202, 288, and 421 mV, respectively. The smaller ΔE values state that BzCl is able to lower the polarization of the battery and accelerate the reaction kinetics of the S species.

The cycling properties at 0.5 C were further measured, and the cells were first tested under different current densities as shown in Figure 1e. The cell with BzCl has a more stable performance under the rate of 0.5 C, exhibiting a high capacity of 914.8 mAh g^{-1} after 25 cycles (the first 25 cycles at different current densities) and 693.2 mAh g^{-1} at the 245th cycle, which corresponds to a capacity decay rate of 0.11% per cycle. In contrast, the control cell shows the capacity of 827 mAh g^{-1} after the activation and 345.2 mAh g^{-1} at the 245th cycle with a capacity decay rate of 0.265% per cycle. Moreover, the coulombic efficiency (CE) of the cell with BzCl is >98% even after 245 cycles, while that without BzCl additive is <90%. The higher CE in the BzCl based cell further demonstrates the complete reaction in the S cathode and stable SEI in the Li metal anode. In addition, the advantages of the BzCl additive were further illustrated in the cycling performance test at 1 C, as shown in Figure S2 (Supporting Information). The cell with BzCl has a discharge capacity of 473.9 mAh g^{-1} after 495 cycles, corresponding to a low capacity decay rate of 0.105% per cycle. However, the control cell without BzCl only delivers discharge capacities of 266.1 mAh g^{-1} after 500 cycles and the capacity decay rate is 0.146%. The charge–discharge curves of the BzCl cell in Figure S2 (Supporting Information) at the 1st, 2nd, 100th, 300th, and 500th cycle are shown in Figure S3 (Supporting Information), which not only show the high retention of the capacities after different cycles, but also exhibit the stable charge and discharge plateaus along with the cycles, proving the positive effect of the BzCl in the S conversion during the long cycles. The performance with high S loading is a key property of the Li–S battery toward practical application for the rising energy density of the overall device. Thus, the cell with BzCl was further evaluated with the S loading of 4 mg cm^{-2} at 0.1 C, which affords a capacity of 828.6 mAh g^{-1} after 130 cycles with a low decay rate of 0.079% (Figure 1f). Even under S loading of 4.5 mg cm^{-2} and low electrolyte/S ratio (E/S) of 10 µL mg^{-1} conditions, the cell using BzCl still provides 763.5 mAh g^{-1} capacity after 110 cycles with decay rate of only 0.142% (Figure S4, Supporting Information). Compared with other reported works of electrolyte additives, our work has superiority in both capacity and stability as shown in Figure 1d and Table S1 (Supporting Information), which indicates the potential of BzCl to develop high-performance Li–S battery.

2.2. Effect of BzCl on the Polysulfide Regulation

In order to figure out the contribution of BzCl to the excellent electrochemical performance during battery operation, we designed an H-type glass cell composed of a Li anode (left side) and a S cathode (right side). As the discharge proceeds, the color of the standard electrolyte in the cathode chamber changes from transparent to light yellow and further to dark yellow due to the continuous dissolution of soluble LiPSs (**Figure 2a**). It is important to note that the yellow LiPSs gradually diffuse to the Li anode side from 1.92 V, demonstrating the serious shuttling of LiPSs in standard electrolyte. In contrast, both cathode and anode chambers with BzCl-contained electrolyte remain transparent during the whole discharge process (Figure 2b), suggesting BzCl can rapidly interact with the LiPSs once the LiPSs dissolve in the electrolyte, thus suppressing the crossover of LiPSs effectively. The absence of LiPSs in anode side of BzCl-contained electrolyte was further verified by UV–vis adsorption spectroscopy. After discharging to 2.1 V, the Li anode was extracted from the disassembled coin cell and immersed into 1,3-dioxolane/1,2-dimethoxyethane (DOL/DME) solution for spectroscopic measurements. As shown in Figure S5 (Supporting Information), a broad peak at 375 nm, corresponding to the soluble LiPSs, is much weaker than that in the standard electrolyte, indicating BzCl is more beneficial for blocking the diffusion of LiPSs from the cathode to the anode.

The good LiPS blocking effect of BzCl can also be confirmed by a static LiPS adsorption test. As shown in Figure S6 and Video S1 (Supporting Information), the original Li_2S_8 solution in bright yellow color becomes colorless upon dropping BzCl, which indicates BzCl has a good adsorption to LiPSs. Moreover, the Raman spectra (Figure 2c) show that, upon addition of BzCl to the DOL/DME with Li_2S_8 solution, the intensities of Li_2S_8-associated peaks (marked with red rhombus) decrease; Meanwhile, a new peak appears at 480 cm^{-1}. These results suggest that LiPSs strongly binds with BzCl through forming chemical bonding. The high chemical affinity of LiPSs with BzCl was further confirmed using ^{7}Li NMR (Figure 2d), where there is an obvious shift between the Li_2S_8 solutions without and with BzCl. Thanks to such a strong chemical interaction between BzCl and LiPSs, the Li–S cell with BzCl shows lower stabilized current (so-called shuttle current), directly proving the positive role of BzCl in mitigating LiPS diffusion and shuttling (Figure 2e).

Sulfur reduction reaction (SRR) kinetics, as a critical aspect affecting battery performance, was further evaluated by cyclic voltammograms (CVs). As illustrated in Figure 2f, the reduction/oxidation peaks in BzCl electrolyte-based cell show greater current intensities and more positive/negative shift, indicating a lower voltage hysteresis and faster S redox kinetics realized by adding BzCl (Figure S7, Supporting Information). The Tafel plots of the redox peaks based on the CV curves (Figure S8, Supporting Information) were calculated to analyze the catalytic activity of different reaction processes, where the cell using BzCl always shows much smaller slopes for the oxidation and reduction peaks, directly reflecting its positive effect toward the accelerated LiPS redox kinetics. This more efficient catalytic effect of BzCl for polysulfide conversion is further confirmed by electrochemical impedance spectroscopy (EIS) in Figure 2g. Typically, the Nyquist plots consist of two depressed semicircles and a linear tail, where the first semicircle represents the resistance of the SEI (R_{SEI}), the second semicircle represents the charge transfer (R_{CT}) for polysulfide conversion, and the point where the plots cross over the x-axis can reflect the conduction processes in the solid/liquid phase (R_S). The cell with BzCl exhibits visibly lower impedances at the initial state and after 30 cycles (initial state: R_S = 2.3 Ω, R_{SEI} = 18.1 Ω, R_{CT} = 6.1 Ω; 30th cycle: R_S = 8.4 Ω, R_{SEI} = 9.3 Ω, R_{CT} = 4.5 Ω) in comparison with the cell without BzCl (initial state: R_S = 6.7 Ω, R_{SEI} = 16.8 Ω, R_{CT} = 9.4 Ω; 30th cycle: R_S = 14.2 Ω, R_{SEI} = 14.7 Ω, R_{CT} = 7.7 Ω) (Figure S9 and Table S2, Supporting Information), demonstrating the stable

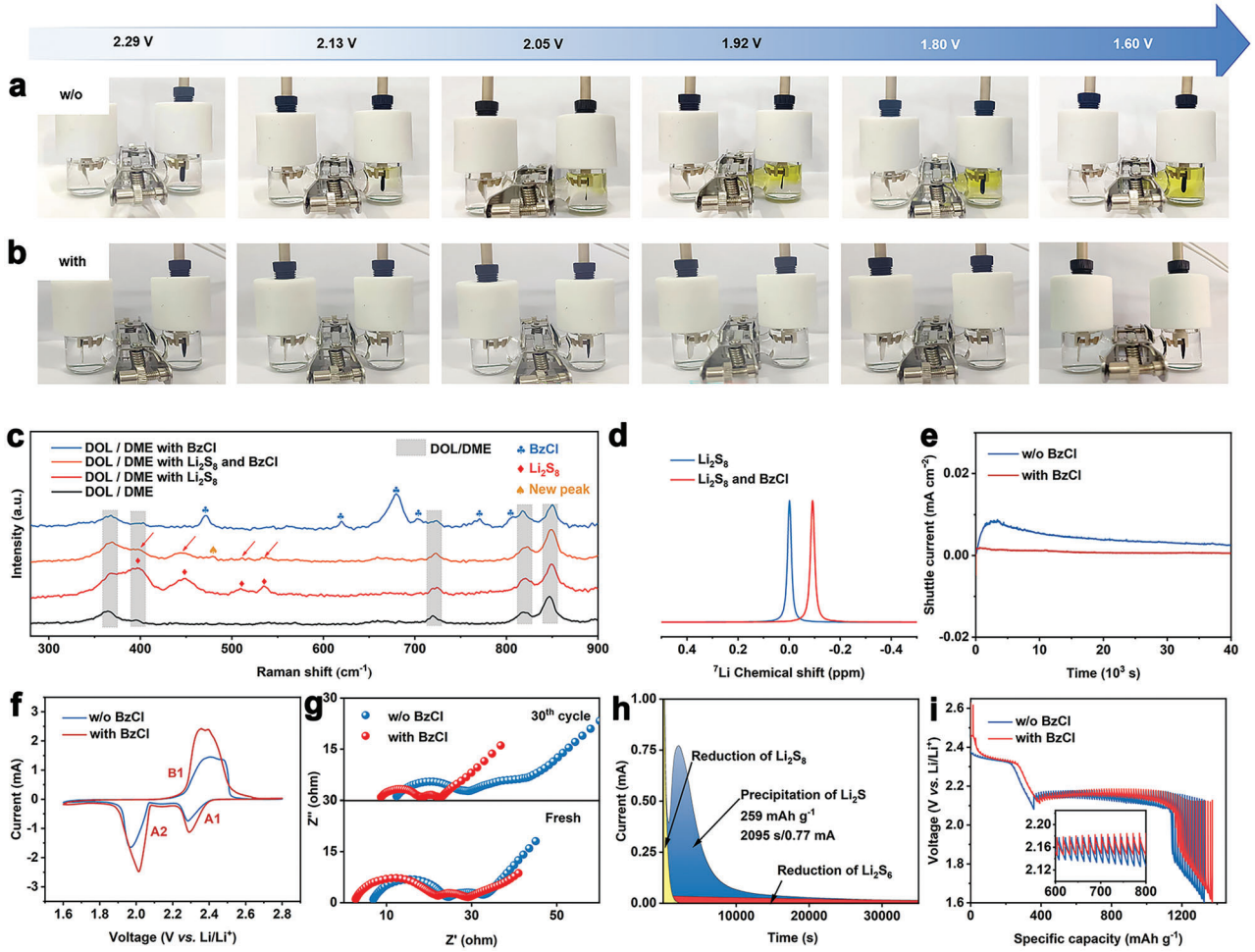

Figure 2. Corresponding photographs of the H-type glass cells a) without and b) with BzCl at different discharge voltages. c) The Raman spectra of the DOL/DME (1:1 vol.%), DOL/DME with Li_2S_8, DOL/DME with BzCl, and DOL/DME with both Li_2S_8 and BzCl. d) The ^{7}Li NMR spectra of Li_2S_8 dissolved in DOL/DME without and with BzCl. e) The shuttle current tests in Li–S cells without and with BzCl. f) The CVs of the Li–S cells without and with BzCl at a scanning rate of 0.1 mV s^{-1}. g) Nyquist plots of the Li–S cells without and with BzCl. h) Potentiostatic discharge and charge profiles of Li_2S nucleation on the electrodes with BzCl. i) The GITT tests of the Li–S cells without and with BzCl.

interphase chemistry and fast kinetics of the battery achieved by BzCl.

The oxidation and reduction processes of Li–S cathode are accompanied by a series of multiphase solid–liquid–solid transition processes. Considering the liquid–solid ($Li_2S_4 \rightarrow Li_2S$) conversion process contributes ≈75% of total capacity, the catalytic effect of BzCl on liquid–solid conversion was quantified through a potentiostatic nucleation test of Li_2S. In this experiment, the cells without and with BzCl were galvanostaticly discharged to 2.06 V, followed by a potentiostatic discharge process at 2.04 V. The potentiostatic nucleation profiles (Figure 2h; Figure S10, Supporting Information) exhibit that the cell with BzCl has greater current intensity (0.77 mA), faster response (2095 s) and higher capacity (259 mAh g^{-1}). In the meantime, the scanning electron microscopy (SEM) characterization and corresponding energy dispersive X-ray spectroscopy (EDS) elemental mappings were shown in Figure S11 (Supporting Information). In the initial CNTs-S electrode, S distributes among the void of CNTs rather than inside the CNT matrix. For the cycled cathode electrodes, it shows that S element is uniformly coated on the CNT skeleton without aggregation in the cell with the presence of the BzCl additive while less and uneven Li_2S deposition forms on the S cathode surface in the control cell. These results suggest that the BzCl can accelerate the deposition of Li_2S, reduce the overpotential of Li_2S conversion, and improve the utilization rate of Li_2S in the battery. The fast liquid–solid conversion kinetics can also be proved by galvanostatic intermittent titration technique (GITT) study, where BzCl cell has much larger variations (IR drop) in equilibrium potential (270–560 mV) than the cell with standard electrolyte (280–790 mV) during the second discharge plateau (Figure 2i).

2.3. Underlying Mechanism on S Cathode with BzCl

Radicals are formed by the homogeneous splitting of covalent bonds in compound molecules under external conditions such as electric field. The strength of chemical bonds and the

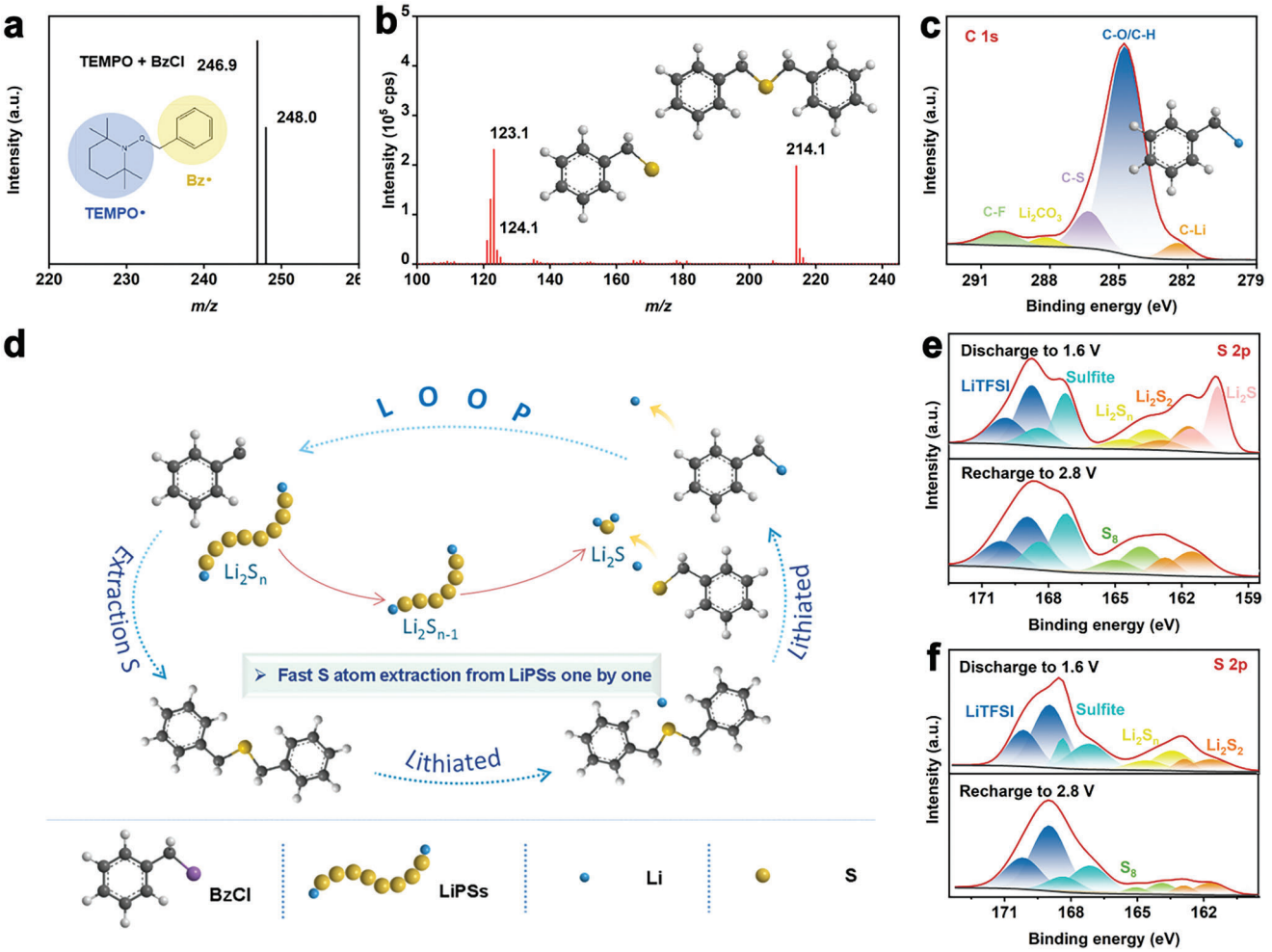

Figure 3. The GC–MS spectra of a) electrolyte with BzCl/TEMPO and b) DOL solution with BzCl/Li_2S_8. c) The C 1s XPS spectra of the fully discharged S cathodes with BzCl additive. d) Reaction mechanism of the multi-step discharge process of the Li–S cell with BzCl. The S 2p XPS spectra of the fully discharged and recharged S cathodes e) with and f) without BzCl.

molecular geometries are important factors affecting the generation and stable existence of radicals. Because the Cl atom in BzCl links the alpha-carbon on the phenyl methyl group by single bond and conjugates with the benzene ring, the C—Cl bond energy is weak, and it is easy to generate stable Bz· radical. Therefore, we validated the form of the BzCl in electrolyte under electric field conditions by adding 2,2,6,6-tetramethylpiperidinooxy (TEMPO) to the electrolyzer as a radical trap (the specific procedure in detail can be found in the Supporting Information). GC–MS spectrum shows that the combination of TEMPO and benzyl group (TEMPO–Bz) is observed, proving the presence of Bz· (**Figure 3a**). GC–MS spectra were further collected to understand the chemical binding between BzCl and LiPSs. As shown in Figure S12 (Supporting Information), there is no significant peak in the spectra of the DOL solution with only BzCl, because BzCl is volatilized before passing through the pyrolysis column. In contrast, the GC–MS spectrum of the DOL with both Li_2S_8 and BzCl show the peaks at 214.3 and 123.1 (Figure 3b), representing to the Bz–S–Bz and Bz–S·. Thus, the chemical binding between BzCl and LiPSs could be speculated to that two Bz· radicals grab a S atom from the LiPSs to finally form Bz–S–Bz. At the meantime, the Cl 2p X-ray photoelectron spectroscopy (XPS) spectra of the cell with BzCl prove that BzCl is enriched in the discharged S electrode (Figure S13, Supporting Information). Moreover, there is a C–Li peak in the C 1s XPS spectrum of the cell with BzCl, which proves that Li^+ is chemically connected to BzCl and probably form BzLi in the electrochemical process (Figure 3c). On account of the above evidences, the reaction process of the S with the BzCl additive can be concluded as the following (Figure 3d): when the S_8 is reduced to LiPSs (e.g., Li_2S_8), the Bz· radicals would interact with the LiPSs and grab a S atom to form B–S–Bz near the cathode surface; with the continuous reduction, Bz–S–Bz combines with the Li^+ and e^- to form lithiated Bz–S–Bz, which splits to Bz–S–Li and Bz–Li rapidly upon the continuous reaction with Li^+ and e^-. Subsequently, the Bz–Li turns to radical Bz· in the electrolyte, while the Bz–S–Li is reduced to form Li_2S and Bz·. On the one hand, the direct formation of Li_2S avoids the rate-determining step, i.e., the conversion from Li_2S_4 to Li_2S_2/Li_2S, and accelerates the rate of the whole SRR. On the other hand, the Bz· radical from both Bz–S–Li and

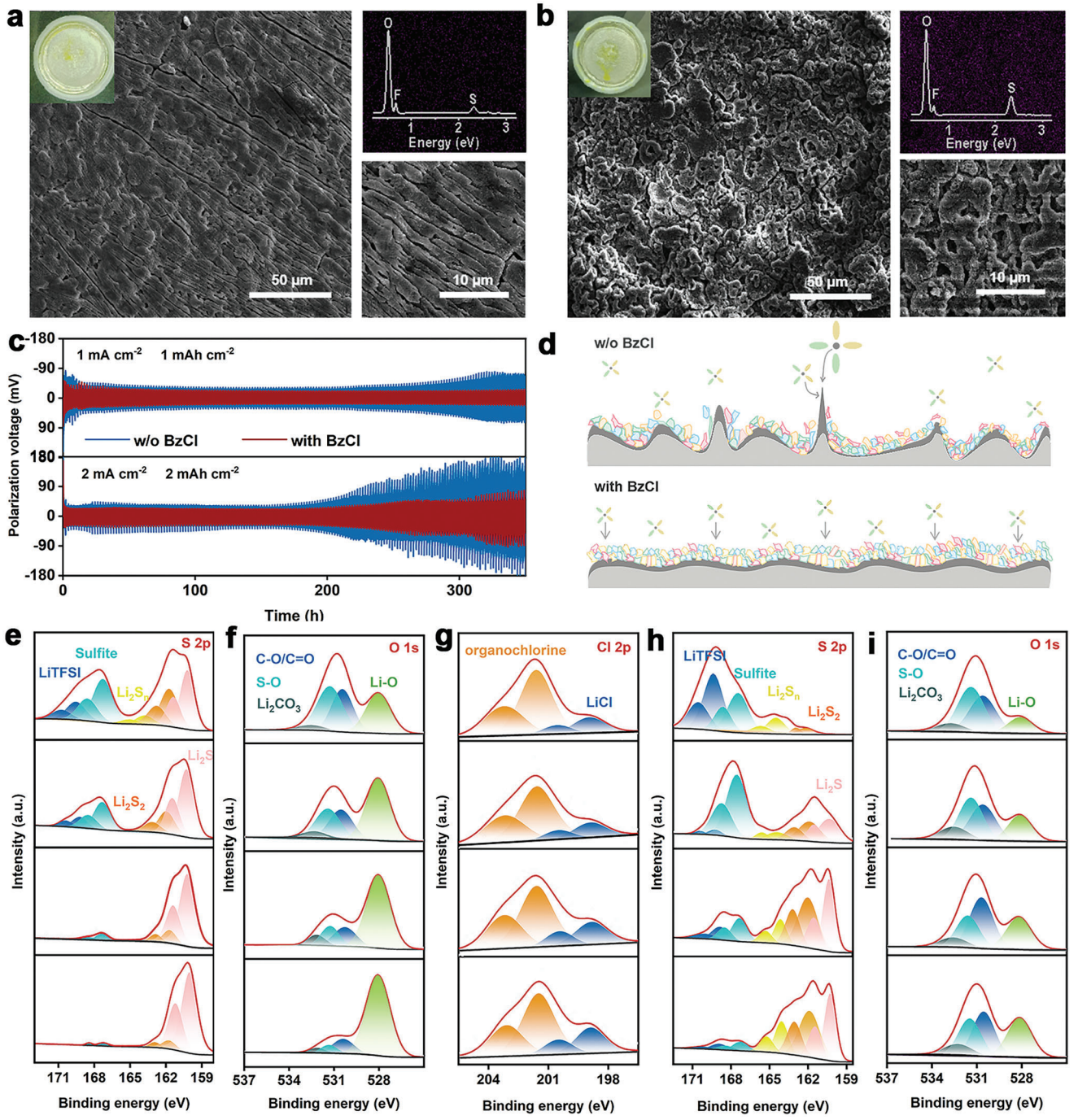

Figure 4. SEM images of the cycled Li anode a) with and b) without BzCl in Li–S cells after 50 cycles. c) Voltage profiles of the different symmetric cells at 1 mA cm^{-2}, 1 mAh cm^{-2}, and 2 mA cm^{-2}, 2 mAh cm^{-2}. d) The schematic diagrams of the two cells on the Li anode. High-resolution XPS spectra with different depth etch on the surface of Li anode: e) S 2p, f) O 1s and g) Cl 2p corresponding to the anode with BzCl, h) S 2p and i) O 1s corresponding to the anode without BzCl.

Bz–Li can further react with LiPSs to form Bz–S–Bz again, forming an electrochemical reaction loop. With this reaction loop, the radical Bz· can keep reacting with LiPSs and break the S in soluble LiPSs, accelerating the LiPSs conversion till the end of the discharge process.

The promotional effect of BzCl toward S conversion can be further confirmed by probing the discharged and recharged products on electrode surface with XPS as shown in Figure 3e,f and Figure S14 (Supporting Information). At the fully discharged state (1.6 V), the cell with BzCl exhibits stronger Li_2S_2 (161.7 eV)/Li_2S (160.2 eV) signals and weaker long-chain LiPS (Li_2S_n, $4 \leq n \leq 8$) signals than the cell with standard electrolyte, suggesting BzCl can better reduce the long-chain LiPSs to short-chain Li_2S_2/Li_2S and accelerate the surface reaction kinetics. This

more efficient electrochemical conversion also happens in S oxidation process, where Li_2S is thoroughly transformed to S_8 in the cell containing BzCl as the cell is recharged back to 2.8 V.

2.4. Mechanism on Li Anode with BzCl

Instability of Li anode is another major barrier to achieving a stable cycling performance in Li–S battery. SEM was used to characterize the surface morphology of the cycled Li anode of the Li–S cells after 50 cycles. As shown in **Figure 4**a, the surface of the Li anode with BzCl possesses plat morphology without Li dendrites. In contrast, Li anode from the standard electrolyte-based cell is clearly observed with incompact structure (Figure 4b). Additionally, the EDS elemental mappings of Li anode with BzCl show that S is uniformly distributed and the intensity of S is obviously lower than that in the standard electrolyte-based cell, further stating that BzCl can effectively alleviate the shuttle of LiPSs and decrease the corrosion of the Li anode. In order to evaluate the effect of BzCl on the Li anode, the Li/Li symmetric cells were comparatively assessed with and without the BzCl additive. (Figure 4c) The cell with BzCl under the current density of 1 mA cm^{-2} and capacity of 1 mAh cm^{-2} shows reversible stability and a stable polarization voltage of 53 mV over 350 h. In contrast, random voltage oscillations occur in the symmetric cell without BzCl after 230 h, and the polarized voltage varies from 71 to 190 mV. Further increasing the current density and capacity to 2 mA cm^{-2} and 2 mAh cm^{-2}, the BzCl electrolyte-based cell still exhibits reversible performance and stable polarization of 70 mA, while the cell with standard electrolyte is deteriorated after 230 h with higher hysteresis of 150 mV, which means continuous growth of Li dendrite puncturing the SEI, causing by the increasing impedance and electrolyte consumption in the standard electrolyte. Oppositely, the stable polarization voltage of the anode with BzCl means the fast kinetics and stable interphase, suggesting BzCl is involved in SEI derivation in much greater depth.

The XPS depth profiling was further implemented to reveal the chemical composition and structure of the SEI on the Li metal after ten cycles of a typical Li–S cells at 0.05 C. A sealed Ar container was used to transfer the cycled Li metal to the XPS chamber to prevent the contamination from air. The surfaces of both Li metals are covered with S species, which are attributed from the shuttled LiPSs reacting with the Li metal as seen in the S 2p in Figure 4e,h. The peaks of Li_2S and Li_2S_2 are dominated in the SEI of the Li metal with BzCl-electrolyte. In contrast, the soluble Li_2S_n is obviously detected in the SEI of the Li metal with standard electrolyte, and the intensities even increase as the depth goes deeper, which imply the formed SEI is loose and porous and prone to accommodate the soluble ingredient. The peaks of LiCl aroused from BzCl and LiF derived from LiTFSI are observed in the SEI with BzCl as shown in Figure 4g and Figure S15 (Supporting Information), proving the formation of an ideal SEI with inorganic components, which is conducive to inhibiting the adverse reaction between the electrolyte and the Li metal anode and improving the ion conductivity and mechanical strength. As the BzCl is not the only film-forming agent, the consumption of a small part of BzCl will have less influence in the performance of the BzCl-based cell. The O 1s spectra for both samples show peaks from 528.1 to 529.0 eV and 531 to 532 eV, which are aligned to the Li_2O as the inorganic ingredients and lithium alkyl carbonate ($ROCO_2Li$), lithium alkoxide (ROLi) as the main organic components (Figure 4f,i). It is noted that the stronger intensity of the Li_2O and weaker intensity of the organic ingredients are found in the BzCl-electrolyte based cell, which is beneficial for the fast ion diffusion and lower resistance. The XPS results of the Li metal anode after circulation demonstrate a robust SEI which is rich in Li_2O and LiF in the BzCl-based cell, and their intensities are higher than those in the standard electrolyte, which is probably due to the use of the exotic additive (BzCl) impeding the solvent effect between the DOL/DME solvent and Li^+, and facilitating the decomposition of LiTFSI in the SEI-forming.[34] The above characterizations suggest that the BzCl additive in electrolyte is in favor of the in situ formed flat and robust SEI layer with fast Li^+ conductivity and high stability (Figure 4d).

3. Conclusion

The role of BzCl in Li–S battery is well analyzed from the perspectives of S conversion and the stable interphase formed in situ on the surface of the Li metal. At the cathode side, BzCl is proved to participate in the electrochemical path of the S evolution, grabbing S atom from the LiPSs to accelerate the redox kinetics due to the unique Bz· radical, alleviating the shuttle effect. Meanwhile, the BzCl helps the formation of a flat and robust SEI with high stability and ion conductivity. As a result, the Li–S battery with BzCl as electrolyte additive exhibits a high capacity and a stable cycling performance. This work proves a simple strategy to overcome the major challenges in Li–S battery from both cathode and anode aspects, providing new means to improve the kinetics and stability by manipulating interfacial chemistry via organic additives.

Supporting Information

Supporting Information is available from the Wiley Online Library or from the author.

Acknowledgements

This research was funded in part by National Natural Science Foundation of China (Grant Nos. 22309135, 22109119, 51972238, and U21A2081), Natural Science Foundation of Zhejiang Province (Grant No. LQ22B030003), Major Scientific and Technological Innovation Project of Wenzhou City (Grant No. ZG2021013).

Conflict of Interest

The authors declare no conflict of interest.

Data Availability Statement

Research data are not shared.

Keywords

lithium deposition, lithium–sulfur battery, organic electrolyte additive, solid electrolyte interphase, sulfur redox reaction

Received: October 31, 2023
Revised: February 8, 2024
Published online:

[1] X. Chen, T. Hou, K. A. Persson, Q. Zhang, *Mater. Today* **2019**, *22*, 142.
[2] D. Lei, K. Shi, H. Ye, Z. Wan, Y. Wang, L. Shen, B. Li, Q.-H. Yang, F. Kang, Y.-B. He, *Adv. Funct. Mater.* **2018**, *28*, 1707570.
[3] Z. Pan, D. J. L. Brett, G. He, I. P. Parkin, *Adv. Energy Mater.* **2022**, *12*, 2103483.
[4] H. Shin, M. Baek, A. Gupta, K. Char, A. Manthiram, J. W. Choi, *Adv. Energy Mater.* **2020**, *10*, 2001456.
[5] C. Yuan, X. Song, P. Zeng, G. Liu, S. Zhou, G. Zhao, H. Li, T. Yan, J. Mao, H. Yang, T. Cheng, J. Wu, L. Zhang, *Nano Energy* **2023**, *110*, 108353.
[6] Z.-J. Zheng, H. Ye, Z.-P. Guo, *Energy Environ. Sci.* **2021**, *14*, 1835.
[7] W. Yao, J. Xu, L. Ma, X. Lu, D. Luo, J. Qian, L. Zhan, I. Manke, C. Yang, P. Adelhelm, R. Chen, *Adv. Mater.* **2023**, *35*, 2212116.
[8] L. Zhou, D. L. Danilov, F. Qiao, J. Wang, H. Li, R.-A. Eichel, P. H. L. Notten, *Adv. Energy Mater.* **2022**, *12*, 2202094.
[9] S. Zhou, S. Yang, X. Ding, Y. Lai, H. Nie, Y. Zhang, D. Chan, H. Duan, S. Yang, S. Huang, Z. Yang, *ACS Nano* **2020**, *14*, 14208.
[10] H. Ye, J. Sun, S. Zhang, H. Lin, T. Zhang, Q. Yao, J. Y. Lee, *ACS Nano* **2019**, *13*, 14208.
[11] Y. Yan, C. Cheng, L. Zhang, Y. Li, J. Lu, *Adv. Energy Mater.* **2019**, *9*, 1900148.
[12] X. Fu, R. Odstrcil, M. Qiu, J. Liu, W.-H. Zhong, *Energy Storage Mater.* **2021**, *42*, 22.
[13] X. Shen, Y. Li, T. Qian, J. Liu, J. Zhou, C. Yan, J. B. Goodenough, *Nat. Commun.* **2019**, *10*, 900.
[14] S. Zhou, W. Chen, J. Shi, G. Li, F. Pei, S. Liu, W. Ye, L. Xiao, M.-S. Wang, D. Wang, Y. Qiao, L. Huang, G.-L. Xu, H.-G. Liao, J.-F. Chen, K. Amine, S.-J. Sun, *Energy Environ. Sci.* **2022**, *15*, 196.
[15] F. Qi, Z. Sun, X. Fan, Z. Wang, Y. Shi, G. Hu, F. Li, *Adv. Energy Mater.* **2021**, *11*, 2100387.
[16] J. Zhang, C. You, H. Lin, J. Wang, *Energy Environ. Mater.* **2022**, *5*, 731.
[17] Y. Lu, J.-L. Qin, T. Shen, Y.-F. Yu, K. Chen, Y.-Z. Hu, J.-N. Liang, M.-X. Gong, J.-J. Zhang, D.-L. Wang, *Adv. Energy Mater.* **2021**, *11*, 2101780.
[18] B. Yan, Y. Li, L. Gao, H. Tao, L. Zhang, S. Zhong, X. Li, X. Yang, *Small* **2022**, *18*, 2107727.
[19] C. Prehal, J.-M. von Mentle, S. Drvaric Talian, A. Vizintin, R. Dominko, H. Amenitsch, L. Porcar, S. A. Freunberger, V. Wood, *Nat. Commun.* **2022**, *13*, 6326.
[20] W. Ren, W. Ma, S. Zhang, B. Tang, *Energy Storage Mater.* **2019**, *23*, 707.
[21] Y. Lin, S. Huang, L. Zhong, S. Wang, D. Han, S. Ren, M. Xiao, Y. Meng, *Energy Storage Mater.* **2021**, *34*, 128.
[22] F. Hippauf, W. Nickel, G.-P. Hao, K. Schwedtmann, L. Giebeler, S. Oswald, L. Borchardt, S. Doerfler, J. J. Weigand, S. Kaskel, *Adv. Mater. Interfaces* **2016**, *3*, 1600508.
[23] H. Ji, Z. Wang, Y. Sun, Y. Zhou, S. Li, J. Zhou, T. Qian, C. Yan, *Adv. Mater.* **2023**, *35*, 2208590.
[24] W. Guo, W. Zhang, Y. Si, D. Wang, Y. Fu, A. Manthiram, *Nat. Commun.* **2021**, *12*, 3031.
[25] A. Gupta, A. Bhargav, A. Manthiram, *ACS Energy Lett.* **2020**, *6*, 224.
[26] S. Kim, Y. M. Kwon, K. Y. Cho, S. Yoon, *Electrochim. Acta* **2021**, *391*, 138927.
[27] S. Yu, S. Yang, D. Cai, H. Nie, X. Zhou, T. Li, C. Liang, H. Wang, Y. Dong, R. Xu, G. Fang, J. Qian, Y. Ge, Y. Hu, Z. Yang, *InfoMat* **2022**, *5*, e12381.
[28] Q. Fan, Y. Si, W. Guo, Y. Fu, *J. Phys. Chem. Lett.* **2021**, *12*, 900.
[29] W. Guo, Z. D. Wawrzyniakowski, M. M. Cerda, A. Bhargav, M. D. Pluth, Y. Ma, Y. Fu, *Chem. Eur. J.* **2017**, *23*, 16941.
[30] J. Sun, K. Zhang, Y. Fu, W. Guo, *Nano Res.* **2022**, *16*, 3814.
[31] S. Li, H. Dai, Y. Li, C. Lai, J. Wang, F. Huo, C. Wang, *Energy Storage Mater.* **2019**, *18*, 222.
[32] G. Naaresh Reddy, R. Parida, S. Giri, *Chem. Commun.* **2017**, *53*, 9942.
[33] A. Kawase, S. Shirai, Y. Yamoto, R. Arakawa, T. Takata, *Phys. Chem. Chem. Phys.* **2014**, *16*, 9344.
[34] R. Meng, X. He, S. J. H. Ong, C. Cui, S. Song, P. Paoprasert, Q. Pang, Z. J. Xu, X. Liang, *Angew. Chem., Int. Ed.* **2023**, *62*, 202309046.